

Components of the dilepton continuum in Pb + Pb collisions at $\sqrt{s_{NN}} = 2.76$ TeVV. Kumar,^{1,2} P. Shukla,^{1,2,*} and R. Vogt^{3,4}¹*Nuclear Physics Division, Bhabha Atomic Research Center, Mumbai, India*²*Homi Bhabha National Institute, Anushakti Nagar, Mumbai, India*³*Physics Division, Lawrence Livermore National Laboratory, Livermore, California 94551, USA*⁴*Physics Department, University of California, Davis, California 95616, USA*

(Received 1 March 2012; revised manuscript received 29 September 2012; published 15 November 2012)

The dilepton invariant mass spectrum measured in heavy-ion collisions includes contributions from important quark-gluon plasma (QGP) probes such as thermal radiation and the quarkonium (J/ψ , ψ' , and Υ) states. Dileptons coming from hard $q\bar{q}$ scattering, the Drell-Yan process, contribute in all mass regions. In heavy-ion colliders, such as the Large Hadron Collider (LHC), semileptonic decays of heavy flavor hadrons provide a substantial contribution to the dilepton continuum. Because the dilepton continuum can provide quantitative information on heavy quark yields and their medium modifications, it is important to identify which dilepton sources populate different parts of the continuum. In the present study, we calculate $c\bar{c}$ and $b\bar{b}$ production and determine their contributions to the dilepton continuum in Pb + Pb collisions at $\sqrt{s_{NN}} = 2.76$ TeV with and without including heavy quark energy loss. We also calculate the rates for Drell-Yan and thermal dilepton production. The contributions to the continuum from these dilepton sources are studied in the kinematic ranges relevant for the LHC detectors. The relatively high p_T cutoff for single leptons excludes most dileptons produced by the thermal medium. Heavy flavors are the dominant source of dilepton production in all the kinematic regimes except at forward rapidities where Drell-Yan dileptons become dominant for masses greater than $10 \text{ GeV}/c^2$.

DOI: [10.1103/PhysRevC.86.054907](https://doi.org/10.1103/PhysRevC.86.054907)

PACS number(s): 12.38.Mh, 24.85.+p, 25.75.-q

I. INTRODUCTION

Heavy-ion collisions study the interaction of matter at the extreme temperatures and densities where a quark-gluon plasma (QGP), a phase of nuclear matter dominated by color degrees of freedom, is expected to form. Experimental efforts in this field began with the CERN Super Proton Synchrotron (SPS) ($\sqrt{s_{NN}} \sim 16\text{--}19 \text{ GeV}$) and evolved with data [1] from the first heavy-ion collider, the Relativistic Heavy Ion Collider (RHIC) at Brookhaven National Laboratory ($\sqrt{s_{NN}} = 200 \text{ GeV}$) in the last decade. The advent of Pb + Pb collisions at $\sqrt{s_{NN}} = 2.76 \text{ TeV}$ at the Large Hadron Collider (LHC) has increased excitement in this field. One of the most striking QGP signals is quarkonium suppression [2]. Quarkonia are identified by their reconstructed mass peaks in the dilepton invariant mass distribution. Below $\sim 12 \text{ GeV}/c^2$, the dilepton distribution includes a number of resonance peaks: ρ , ω , and ϕ at low masses and the ψ and Υ states at higher masses. At $91 \text{ GeV}/c^2$, the $Z^0 \rightarrow l^+l^-$ peak appears. The continuum beneath these resonances is primarily composed of leptons from semileptonic decays of heavy flavor hadrons. These heavy flavor decays not only contribute to the resonance background but are important physics signals in their own right [3–8]. The continuum yields in Pb + Pb collisions compared to those in pp collisions can provide information about the medium properties. This makes it important to know the various contributions to the dilepton continuum in different kinematic regimes.

The first measurements of the dilepton spectra at the LHC have recently been reported [9–11]. The CMS experiment

reported the first measurements of the Z^0 mass region in Pb + Pb collisions [9] as well as measurements of the full dimuon distribution, including quarkonia [10]. ATLAS has also reported J/ψ and Z^0 measurements in the dimuon channel [11]. The second LHC Pb + Pb run, at much higher luminosity, has provided higher statistics measurements of the dilepton spectra over the full available phase space. With the measurement of dilepton spectrum in Pb + Pb collisions at the LHC, it is time to reexamine the continuum contributions to the dilepton mass spectrum. The production cross sections of $c\bar{c}$ and $b\bar{b}$ pairs at $\sqrt{s_{NN}} = 2.76 \text{ TeV}$ are calculated to next-to-leading order (NLO) and their correlated contributions to the dilepton continuum are subsequently obtained. We also include the effect of energy loss of charm and bottom quarks in the medium consistent with measurements of the suppression factor R_{AA} on the lepton spectra from semileptonic decays of charm and bottom quarks [12,13]. These contributions are compared to direct dilepton production from the Drell-Yan process and from thermal production in the medium. We then evaluate the relative importance of these contributions in the LHC detector acceptances.

While there have been previous studies of Pb + Pb collisions at 5.5 TeV [4,6,14], a re-examination is appropriate at the current, lower, center-of-mass energy and with the final detector acceptances. In addition, updated parametrizations of the parton distribution functions as well as estimates of the effect of energy loss on single-particle spectra and determinations of the initial temperature from the charged-particle multiplicity are now available and should lead to improved predictions. The experimental dilepton measurements presently concentrate on resonances. However, background-subtracted dilepton continuum measurements should soon be available with good statistics at 2.76 TeV in both pp and Pb + Pb collisions, which

* pshukla@barc.gov.in

could be used to infer properties of the medium produced in Pb + Pb collisions.

II. DILEPTON PRODUCTION BY HARD PROCESSES

Dilepton production from semileptonic decays of $D\bar{D}$ (charm) and $B\bar{B}$ (bottom) meson pairs has been an area of active theoretical [4,5,7,15,16] and experimental [17] research. The large heavy quark mass allows their production to be calculated in perturbative QCD. We calculate the production cross sections for $c\bar{c}$ and $b\bar{b}$ pairs to NLO in pQCD [4,5] using the CTEQ6M parton densities [18]. The central EPS09 parameter set [19] is used to calculate the modifications of the parton densities in Pb + Pb collisions.

We include the theoretical uncertainty bands on charm and bottom production following the method of Ref. [20]. We use the same set of parameters as that of Ref. [20] with the exclusive NLO calculation of Ref. [21] to obtain the exclusive $Q\bar{Q}$ pair rates as well as their decays to dileptons. We take $m_c = 1.5 \text{ GeV}/c^2$, $\mu_F/m_T = \mu_R/m_T = 1$ and $m_b = 4.75 \text{ GeV}/c^2$, $\mu_F/m_T = \mu_R/m_T = 1$ as the central values for charm and bottom production respectively. Here μ_F is the factorization scale, μ_R is the renormalization scale, and $m_T = \sqrt{m^2 + p_T^2}$. The mass and scale variations are added in quadrature to obtain the uncertainty bands [20].

Figure 1 shows the uncertainty bands on the p_T and rapidity distributions of charm and bottom quarks in Pb + Pb collisions at $\sqrt{s_{NN}} = 2.76 \text{ TeV}$ with shadowing effects included. We only calculate the uncertainties in the production cross sections due to the mass and scale parameters and not those due to the EPS09 modifications or those of the parton densities. Both of these uncertainties are smaller than those due to the choice of mass and scale [22], particularly for $p_T \geq m$. The uncertainties on the heavy flavor production cross sections can be rather large; see Refs. [23,24]. Thus the relative charm and bottom rates at 2.76 TeV may vary by a factor of 2 or more before dense-matter effects such as energy loss are taken into account.

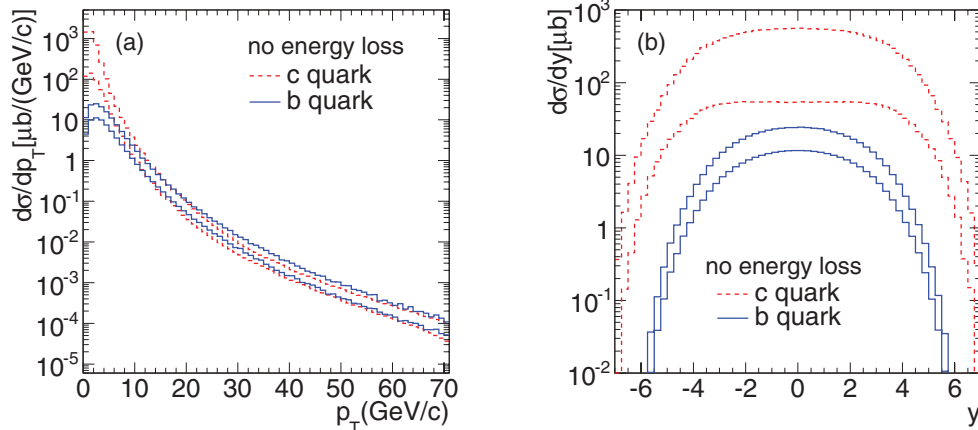


FIG. 1. (Color online) Theoretical uncertainty bands on inclusive single charm and bottom quark production cross sections per nucleon as functions of p_T (left) and rapidity (right) for $\sqrt{s_{NN}} = 2.76 \text{ TeV}$. The uncertainties are calculated by varying the quark mass, renormalization scale μ_R , and factorization scale μ_F . The calculations include modification of the initial parton distributions with the EPS09 central parameter set. No final-state energy loss is included.

TABLE I. Heavy flavor and Drell-Yan cross sections at $\sqrt{s_{NN}} = 2.76 \text{ TeV}$. The cross sections are given per nucleon while $N_{Q\bar{Q}}$ and N_{l+l-} are the number of $Q\bar{Q}$ and lepton pairs per Pb + Pb event. The uncertainties in the heavy flavor cross section are based on the Pb + Pb central values with the mass and scale uncertainties added in quadrature.

	$c\bar{c}$	$b\bar{b}$	DY $1 \leq M \leq 100 \text{ GeV}$
σ_{PbPb}	$1.76^{+2.32}_{-1.29} \text{ mb}$	$89.3^{+42.7}_{-27.2} \mu\text{b}$	70.97 nb
$N_{Q\bar{Q}}$	$9.95^{+13.10}_{-7.30}$	$0.50^{+0.25}_{-0.15}$	
$N_{\mu+\mu-}$	$0.106^{+0.238}_{-0.078}$	$0.0059^{+0.0029}_{-0.0017}$	0.0004

While a recent reevaluation of the mass and scale parameters used to calculate charm production shows that the uncertainty on the charm production cross section can be reduced, it cannot be eliminated [22].

The differences in the quark p_T distributions are primarily at low p_T . For $p_T > 10 \text{ GeV}/c$, the uncertainty bands overlap almost completely with the upper limit on the bottom production band somewhat above the charm upper limit for $p_T > 20 \text{ GeV}/c$. The widths of the rapidity distributions are limited by the heavy quark mass. Thus the charm quark rapidity distribution is broader than that for bottom quarks. The uncertainty bands are broader in rapidity than in p_T for charm quarks and the bands for the two flavors are cleanly separated because the p_T -integrated rapidity distribution is dominated by low p_T , where the charm cross section is clearly greater and the scale uncertainties are larger.

The production cross sections for heavy flavor and Drell-Yan dileptons at $\sqrt{s_{NN}} = 2.76 \text{ TeV}$ are shown in Table I. The number of $Q\bar{Q}$ pairs in a minimum-bias Pb + Pb event is obtained from the per-nucleon cross section, σ_{PbPb} , by

$$N_{Q\bar{Q}} = \frac{A^2 \sigma_{\text{PbPb}}^{Q\bar{Q}}}{\sigma_{\text{PbPb}}^{\text{tot}}} . \quad (1)$$

At 2.76 TeV, the total Pb+Pb cross section, $\sigma_{\text{PbPb}}^{\text{tot}}$, is 7.65 b [25].

We assume that all the observed heavy flavor production in Pb + Pb collisions occurs during the initial nucleon-nucleon collisions. Thermal production of $Q\bar{Q}$ pairs is expected to be only a fraction of this initial production [4] unless the plasma is composed of massive quasiparticles, which would lower the effective threshold for heavy flavor production in the medium [26], enhancing production in this channel. However, such production would be at lower transverse momentum and with a narrower rapidity distribution than shown in Fig. 3.

The heavy quarks decay semileptonically and lepton pairs are formed from correlated $Q\bar{Q}$ pair decays. We do not consider uncorrelated $Q\bar{Q}$ contributions to the continuum since these should be eliminated by a like-sign subtraction. We assume that any uncorrelated dileptons from $c\bar{b}$ and $\bar{c}b$ decays are also removed by like-sign subtraction and that lepton pairs from a single chain decay, $B \rightarrow Dl_1X \rightarrow l_1l_2X'$, only contribute to the low mass continuum; see Ref. [6]. The number of lepton pairs is obtained from the number of $Q\bar{Q}$ pairs,

$$N_{\mu^+\mu^-} = N_{Q\bar{Q}}[B(Q \rightarrow lX)]^2. \quad (2)$$

The values of $N_{Q\bar{Q}}$ and $N_{\mu^+\mu^-}$ are given in Table I, along with their uncertainties.

Dilepton production by the Drell-Yan process has also been calculated to NLO in pQCD [27]. The cross section in the mass interval $1 < M < 100$ GeV, including EPS09 shadowing in Pb+Pb collisions, is given in Table I. The integrated cross section is dominated by the lowest masses. The largest potential modification due to the presence of the nucleus is on the low mass rate, in the resonance region. At larger masses, this effect becomes competitive with the effects of the relative number of protons and neutrons in the nucleus compared to a pp collision (isospin effects) [28]. We have used PYTHIA [29] to generate the Drell-Yan p_T distribution and to place kinematic cuts on the individual leptons of the pair. The total rate has been normalized to the calculated

NLO cross section. The pQCD uncertainties on the Drell-Yan rate, particularly above the resonance region, are not large. In general, they are smaller than the uncertainties due to the shadowing parametrization [28].

Finally, we include energy loss effects on the charm and bottom quarks. Since heavy quarks do not decay until after they have traversed the medium, their contribution to the final dilepton spectra will reflect its influence. Indications from inclusive nonphotonic lepton spectra at RHIC [12], attributed to heavy flavor decays, suggest that the effects of energy loss are strong and persist up to high p_T . They also suggest that the magnitude of the loss is similar for that of light flavors, i.e., independent of the quark mass so that the effects are similar for charm and bottom quarks. The source of this loss as well as its magnitude are still under investigation; see Ref. [30] and references therein.

To estimate the effects of energy loss on the dilepton continuum, we adjust the heavy quark fragmentation functions to give a value of R_{AA} for each flavor separately that is consistent with the measured prompt lepton R_{AA} in central Pb+Pb collisions at high p_T , $R_{AA} \sim 0.25\text{--}0.30$ [13], for both charm and bottom quarks. We then use these modified fragmentation functions to calculate the medium-modified dilepton distributions from heavy flavor decays.

Including energy loss does not change the total cross section since it moves the quarks to lower momentum without removing them from the system. Thus the p_T -integrated rapidity distributions are also unaffected, see Fig. 2, which presents the single inclusive heavy flavor production uncertainty bands after energy loss. The charm and bottom quark p_T distributions still exhibit the same general behavior: the slopes are parallel to those without energy loss at high p_T but show a pileup of low- p_T quarks after loss is included. After taking energy loss into account, the point where the bottom quark distribution begins to dominate is shifted to lower p_T , ~ 10 GeV/ c instead of ~ 20 GeV/ c when the widths of the bands are accounted for.

The relative strength of charm and bottom quark energy loss in the medium is not yet settled. Although bottom quarks

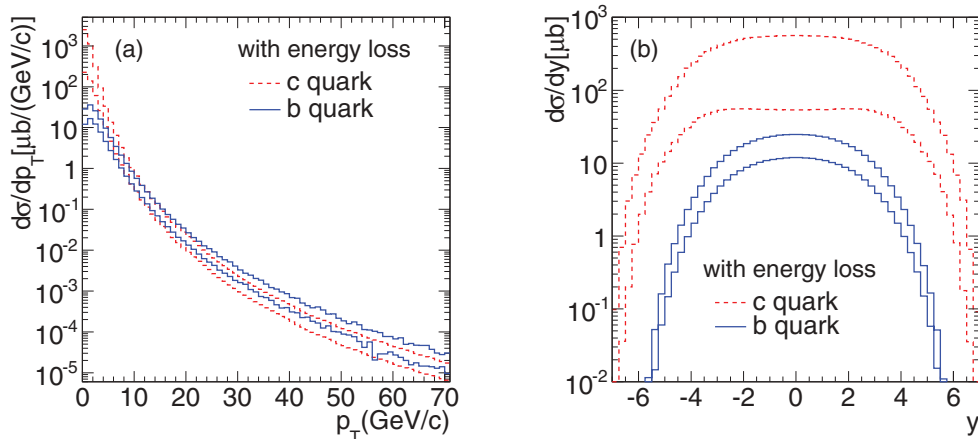


FIG. 2. (Color online) Theoretical uncertainty bands on inclusive single charm and bottom quark production cross sections per nucleon as functions of p_T (left) and rapidity (right) for $\sqrt{s_{NN}} = 2.76$ TeV. The uncertainties are calculated by varying the quark mass, renormalization scale μ_R , and factorization scale μ_F . The calculations include modification of the initial parton distributions with the EPS09 central parameter set. Here we include final-state energy loss assuming that the charm and bottom quark R_{AA} is the same, as discussed in the text.

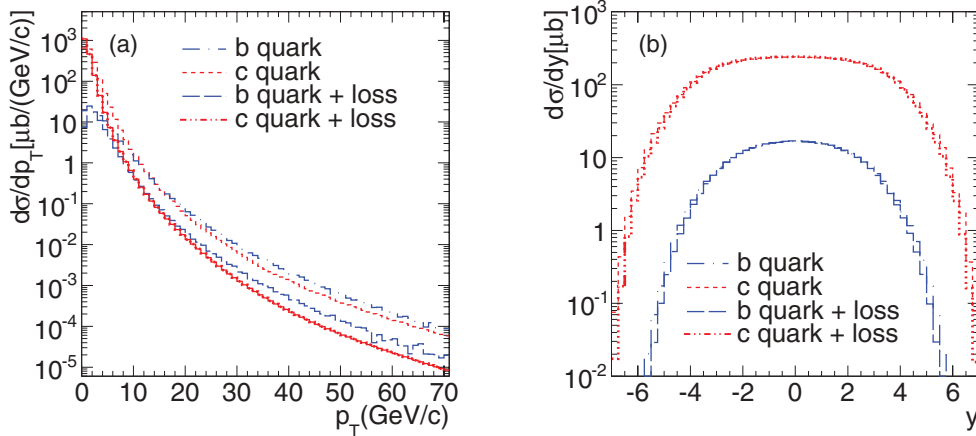


FIG. 3. (Color online) The inclusive single charm and bottom quark per nucleon cross sections as a function of p_T (left) and rapidity (right) both with and without energy loss in Pb + Pb collisions at $\sqrt{s_{NN}} = 2.76$ TeV. The cross sections, given per nucleon, include modification of the initial parton distributions via the central EPS09 shadowing parametrization.

are expected to lose less energy than charm quarks, the data from RHIC and LHC exhibit important differences [31,32]. If we assume that bottom quarks lose less energy than charm quarks, then the bottom and charm quark uncertainty bands in Fig. 2 will separate at high p_T with the bottom quark band above that of the charm quark.

Figure 3 compares the central values of the uncertainty bands with and without energy loss directly. We note that the difference in the heavy flavor p_T distributions due to energy loss is larger than the uncertainty bands with and without energy loss. The rapidity distributions do not show any significant effect due to energy loss since the results are shown integrated over all p_T . Since the total cross sections are unchanged without any acceptance cuts, there is an effect only at far forward rapidity.

III. THERMAL DILEPTON PRODUCTION

The contribution of thermal dileptons is calculated assuming that a QGP is formed in local thermal equilibrium at some initial temperature T_i and initial time τ_i which cools hydrodynamically through a one-dimensional (1D) Bjorken expansion [33]. Assuming a first-order phase transition, when the QGP cools to the critical temperature T_c at time τ_c , the temperature of the system is held fixed until hadronization is completed at time τ_h . Afterwards, the hadron gas cools to the freeze-out temperature T_f at time τ_f [34].

The thermal dilepton emission rate due to $q\bar{q} \rightarrow l^-l^+$ is [34,35]

$$\begin{aligned} \frac{dN}{d^4x d^2p_T dy dM^2} &= \frac{3}{(2\pi)^5} M^2 \sigma(M^2) F \exp(-E/T) \\ &= \frac{\alpha^2}{8\pi^4} F \exp(-E/T). \end{aligned} \quad (3)$$

Here M , p_T , and y are the mass, transverse momentum, and rapidity of the lepton pair while $d^4x = \tau d\tau \eta\pi R_A^2$, where η is the rapidity of the fluid with temperature T and $R_A = r_0 A^{1/3}$. The mass-dependent cross section $\sigma(M^2) = F4\pi\alpha^2/3M^2$

includes a factor F that depends on the phase of the matter. In a two-flavor QGP, $F_{\text{QGP}} = \sum e_q^2 = 5/9$, while, in the hadronic phase, form factors representing the resonance region [36] are used. We concentrate on masses above the resonance region. In the mixed phase,

$$F = [1 - h(\tau)] F_{\text{QGP}} + h(\tau) F_{\text{had}}, \quad (4)$$

where $h(\tau)$ is the hadron fraction of the mixed phase.

The dilepton p_T distribution is

$$\begin{aligned} \frac{dN}{d^4x dy dM dp_T} &= \frac{\alpha^2}{4\pi^4} F M p_T \\ &\times \exp\left(-\frac{\sqrt{M^2 + p_T^2} \cosh(y - \eta)}{T}\right) \end{aligned} \quad (5)$$

and the dilepton invariant mass distribution, integrated over p_T , is

$$\frac{dN}{d^4x dy dM} = \frac{\alpha^2}{2\pi^3} F M^3 \left(\frac{1}{x^2} + \frac{1}{x}\right) \exp(-x), \quad (6)$$

where

$$x = \frac{M \cosh(y - \eta)}{T}. \quad (7)$$

The initial time is assumed to be $\tau_i = 0.1$ fm/c. The initial temperature T_i is obtained from the total multiplicity distribution,

$$\frac{dN}{dy} = \tau_i T_i^3 4a_q \pi R_A^2 / 3.6, \quad (8)$$

where $dN/dy = 1.5(dN_{\text{ch}}/dy)$. The charged-particle multiplicity, $dN_{\text{ch}}/dy = 1600$, was measured in Pb + Pb collisions at 2.76 TeV [37]. Using this value with $a_q = 37\pi^2/90$ gives $T_i = 636$ MeV. The temperature decreases in the QGP as

$$T(\tau) = T_i \left(\frac{\tau_i}{\tau}\right)^{1/3} \quad (9)$$

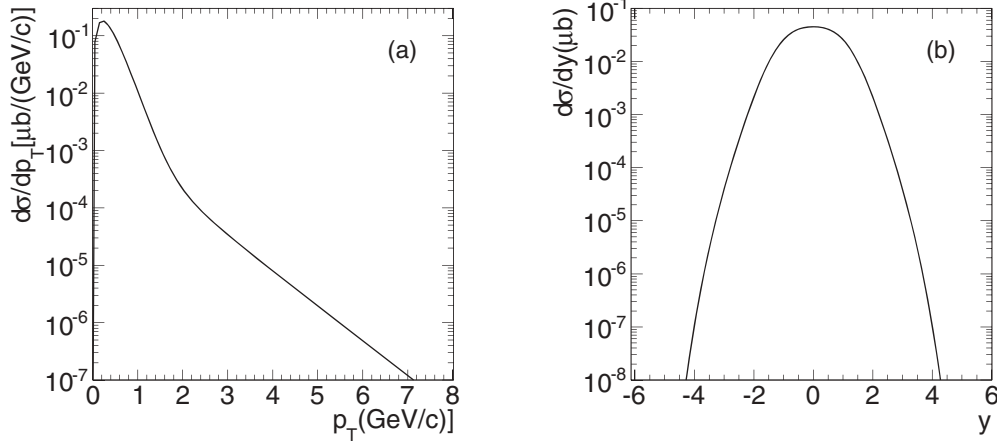


FIG. 4. The thermal dilepton cross section as a function of p_T (left) and rapidity (right) in Pb + Pb collisions at $\sqrt{s_{NN}} = 2.76$ TeV.

for $\tau_i < \tau < \tau_c$. The temperature in mixed phase is $T = T_c = 160$ MeV. The mixed phase ends at $\tau_h = (a_q/a_h)\tau_c$ where $a_h = 3\pi^2/90$ for a pion gas. The hadronic fraction of the mixed phase, $h(\tau)$, is

$$h(\tau) = \frac{a_q}{a_q - a_h} \left(\frac{\tau - \tau_c}{\tau} \right). \quad (10)$$

The temperature in hadron phase between $\tau_h < \tau < \tau_f$, is

$$T(\tau) = T_c \left(\frac{\tau_h}{\tau} \right)^{1/3}. \quad (11)$$

The thermal dilepton rate given in Eqs. (5) and (6) is converted to a cross section by dividing the rate by the minimum bias nuclear overlap, T_{PbPb} . Figures 4(a) and 4(b) show the differential cross sections for thermal dilepton production as a function of p_T and rapidity. The p_T distribution, integrated over pair mass, shows two slopes, a steep decrease when the minimum pair transverse mass, M_T , is on the order of the temperature and a long tail when $M_T \gg T$. The rapidity distribution is significantly narrower than those resulting from the initial hard scatterings shown in Fig. 3.

This simple application of a one-dimensional Bjorken expansion through a first-order phase transition significantly overestimates the lifetime of the hot system. Thus, the results shown in Fig. 4 should be regarded as an upper limit on the thermal contribution.

To obtain the pair mass distributions with single lepton cuts, single leptons are generated by sampling the pair M , p_T , and y distributions, employing a Monte Carlo simulation and accounting for energy-momentum conservation.

IV. RESULTS AND DISCUSSION

In Fig. 5, we show the theoretical uncertainty bands on the dilepton invariant mass distributions from semileptonic charm and bottom decays. The uncertainty bands for the decay dileptons are calculated identically to those of the charm and bottom quark distributions shown in Sec. II. The dilepton uncertainty bands are broader than those for the single inclusive heavy flavors and, here, the dilepton band from charm quarks decays is wider than for bottom quarks. This is the case both without, Fig. 5(a), and with, Fig. 5(b),

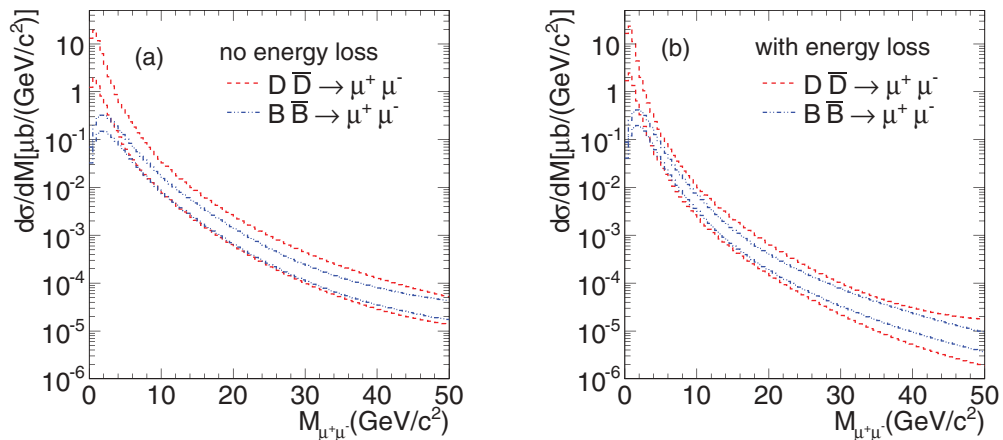


FIG. 5. (Color online) Theoretical uncertainty bands for the dilepton invariant mass distributions from semileptonic charm (red, short-dashed) and bottom (blue, dot-dot-dashed) decays. The uncertainties are calculated the same way as in Sec. II.

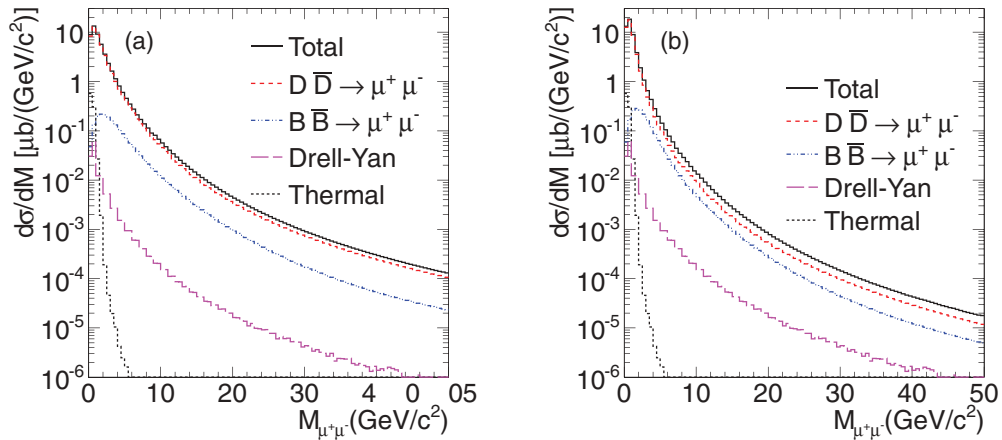


FIG. 6. (Color online) The invariant mass distributions for the four contributions to the dilepton spectra discussed here: semileptonic charm (red, short-dashed) and bottom (blue, dot-dot-dashed) decays, and Drell-Yan (magenta, long-dashed) and thermal (black, dotted) dileptons along with the sum (black, solid) in Pb + Pb collisions per nucleon pair at $\sqrt{s_{NN}} = 2.76$ TeV. The left panel shows distributions without any final-state energy loss; the right panel is after including heavy quark energy loss in the medium. The per-nucleon cross sections are given. No phase space or kinematic cuts are introduced.

energy loss. While we show only the central values of these distributions in the remainder of this section, it is important to keep in mind the significant mass and scale uncertainties in heavy flavor production, considerably larger than those in high mass Drell-Yan production.

Figure 6 shows the dimuon invariant mass distributions from each of the four sources considered: semileptonic decays of correlated $Q\bar{Q}$ pairs and direct production of Drell-Yan and thermal dileptons in Pb + Pb collisions at $\sqrt{s_{NN}} = 2.76$ TeV. Figure 6(a) shows the heavy flavor mass distributions without any final-state energy loss while energy loss is included in the heavy flavor distributions on Fig. 6(b). Only the central values of the heavy flavor contributions are shown. The Drell-Yan and thermal dilepton distributions are unchanged. No kinematic cuts are included. Without cuts, dileptons from $D\bar{D}$ decays dominate over the entire mass range due to the large $c\bar{c}$ production cross section. Bottom pair decays are the next largest contribution followed by Drell-Yan production. At masses below 3 GeV/c², the Drell-Yan and thermal dilepton contributions are competitive. Otherwise, the thermal contribution is negligible. Including energy loss steepens the slope of the heavy flavor mass distributions and also moves the $D\bar{D}$ decay distributions closer to the $B\bar{B}$ decay distributions. In the remainder of this section, we will show only results with final-state heavy flavor energy loss included.

We now examine these distributions in the kinematic regimes appropriate for the LHC detectors. CMS [38] and ATLAS [39] have excellent muon detectors with similar coverage in the central rapidity region, $|\eta^\mu| \leq 2.4$. However, due to the large magnetic fields, only muons above a rather high minimum p_T , $p_T > 3.0$ GeV/c, make it into the muon detectors. ALICE [40] has muon acceptance on one side of the forward rapidity region, $2.5 \leq \eta^\mu \leq 4.0$. At central rapidities, $|\eta^\mu| \leq 1.0$, ALICE has an electron detector. Some previous studies of Pb + Pb collisions at 5.5 TeV, using leading-order calculations of heavy quark production and assuming significantly higher initial temperatures than employed here,

suggested that thermal dileptons could be extracted from the QGP [14]. Thus they reached different conclusions about the relative contributions of thermal and heavy flavor dileptons to the continuum.

Figure 7 shows the dimuon invariant mass distribution for single muons in the range $|\eta^\mu| \leq 2.4$, together with several muon p_T cuts. Figure 7(a) has no muon p_T cut, only the η cut. Comparison with Fig. 6 shows that the thermal dilepton contribution is almost unaffected since its rapidity distribution is sufficiently narrow to fit within the CMS rapidity acceptance. Since the Drell-Yan rapidity distribution narrows with increasing mass, only the low mass region is affected by the rather broad rapidity cut of $|\eta^\mu| \leq 2.4$. Because the charm rapidity range is broader than that of bottom production, the dileptons from charm decays are most affected by the rapidity cut. For $M_{\mu^+\mu^-} > 5$ GeV/c², the charm dilepton yield has dropped below that of bottom quarks.

Adding a cut on single lepton p_T disproportionately affects the low mass part of the continuum. As the minimum lepton p_T is increased from 1 to 10 GeV/c in Figs. 7(b)–7(d), an ever-deepening dip appears in the dilepton mass distribution for $M_{\mu^+\mu^-} < 2p_T^\mu$. Even a relatively low p_T cut essentially eliminates the thermal dilepton contribution since these leptons have a rather soft p_T distribution. Since the charm and bottom quark p_T distributions have the same slope for $p_T > 7$ GeV/c, their decays are affected the same way by the lepton p_T cut. Finally, the single lepton cut of $p_T^\mu > 10$ GeV/c, published with the CMS Z^0 measurement [9], based on approximately 50 million events, had a very low continuum background. This is in agreement with the result in Fig. 7(d) which shows that, with energy loss included, the Drell-Yan process is now the dominant contribution to the continuum.

Figure 8 shows the dimuon mass distribution in the narrower central rapidity interval, $|\eta^\mu| \leq 0.8$, equivalent to the muon acceptance in the CMS barrel region and similar to the ALICE electron acceptance, $|\eta^e| \leq 1.0$. Figure 8(a) shows the dimuon distribution before any p_T cut. In this case, the mass

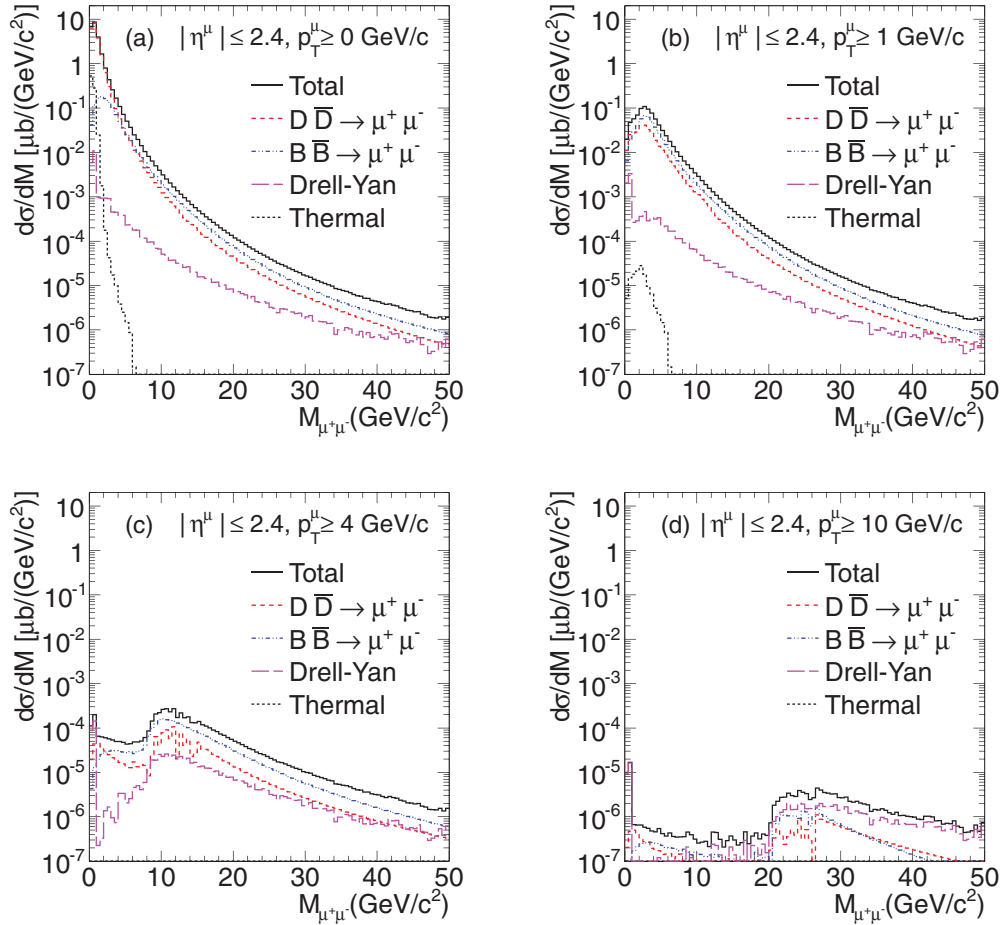


FIG. 7. (Color online) The same as Fig. 6 but now with single muon rapidity cuts of $|\eta^\mu| \leq 2.4$. A minimum single lepton transverse momentum cut of $p_T^\mu \geq 0$ (a), 1 (b), 4 (c), and 10 (d) GeV/c is also shown.

distribution is more steeply falling in all cases except for thermal dilepton production because of its narrow rapidity distribution. Since the heavy flavor hadrons decay isotropically to leptons, the rapidity distribution for lepton pairs is rather broad with a width that is not strongly dependent on the

pair mass. Thus the narrower rapidity acceptance reduces the high mass yields substantially relative to Fig. 7, even before any single lepton p_T cuts. Adding a single lepton transverse momentum cut of $p_T^\mu > 3$ GeV/c, Fig. 8(b), suppresses the low mass part of the distribution. However, the mass

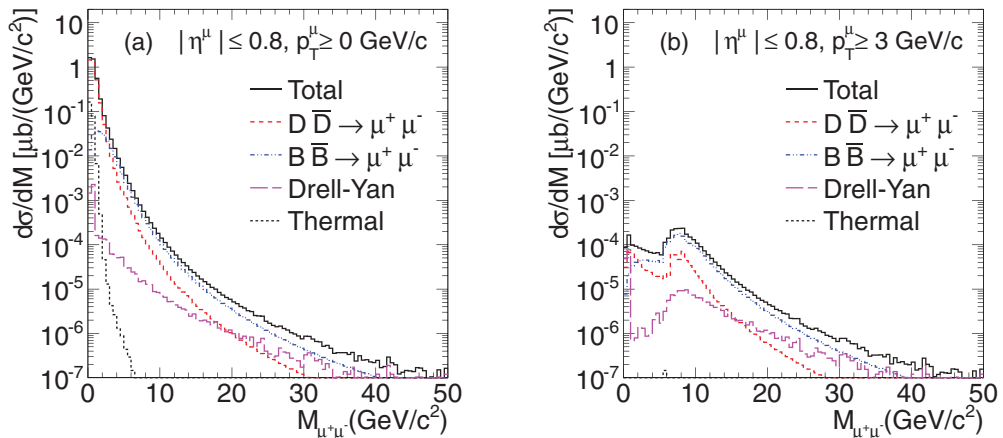


FIG. 8. (Color online) The same as Fig. 6 but now with single muon rapidity cuts of $|\eta^\mu| \leq 0.8$. A minimum single lepton transverse momentum cut of $p_T^\mu \geq 0$ (a) and 3 (b) GeV/c is also shown.

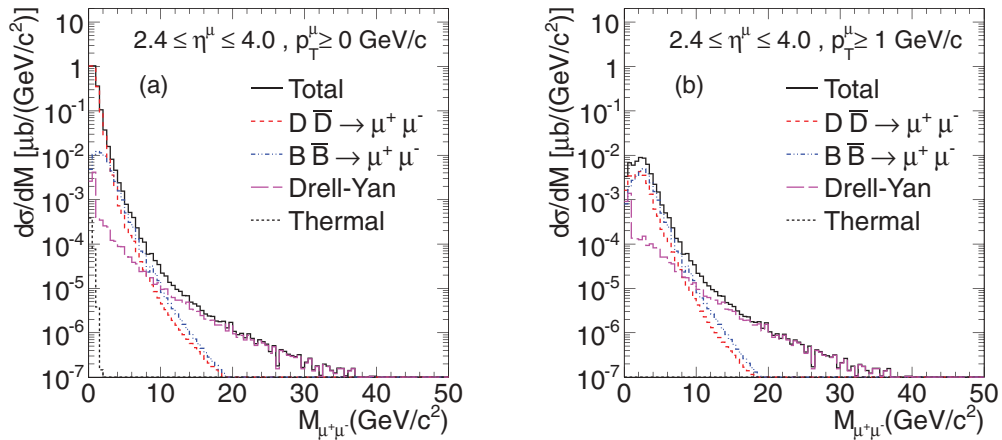


FIG. 9. (Color online) The same as Fig. 6 but now with single muon rapidity cuts of $2.4 \leq |\eta^\mu| \leq 4$. A minimum single lepton transverse momentum cut of $p_T^\mu \geq 0$ (a) and 1 (b) GeV/c is also shown.

distribution is essentially unaffected by the p_T^μ cuts for $M_{\mu^+\mu^-} > 8$ GeV/c².

Figure 9 shows the dimuon mass distributions in the forward region, $2.5 \leq \eta^\mu \leq 4.0$, relevant for the ALICE muon arm. In this case, after energy loss, the Drell-Yan cross section rises above the heavy flavor decay rate for $M_{\mu^+\mu^-} > 10$ GeV/c². The heavy flavor production kinematics favors central production, with a rather steep decrease in the rapidity distribution as the kinematic limit is approached. There is no such constraint on the resulting lepton pairs. Because the decay of the individual heavy quark is isotropic in its rest frame, the lepton rapidity distribution has a larger plateau region, extending to more forward rapidity than the parent quark. However, restricting the cut to one side of midrapidity eliminates many large gap pairs that might survive with a broad central rapidity acceptance such as in Fig. 7. Very little remains of the thermal dilepton contribution in the forward region due to its narrow rapidity distribution.

V. CONCLUSIONS

In summary, we calculate open charm and bottom production and determine their contributions to the dilepton continuum in Pb + Pb collisions at $\sqrt{s_{NN}} = 2.76$ TeV with and without including heavy quark energy loss. These rates are then compared with Drell-Yan and thermal dilepton production. The contributions of all these sources are obtained in kinematic regions relevant for the LHC detectors.

Since most detectors accept only high- p_T single leptons, thermal dileptons would be difficult to measure. Heavy flavors are the dominant source of dileptons in most kinematic regimes, even after energy loss. At forward rapidity, the Drell-Yan contribution begins to dominate for $M > 10$ GeV/c². The effects of energy loss on the decay dileptons alters their acceptance, particularly for high lepton p_T cuts. In most of the kinematic regions considered, the $b\bar{b}$ decay contributions become larger than those of $c\bar{c}$ for lepton pair masses greater than 7 GeV/c².

From the approximately 5×10^7 events collected by CMS in the first year of Pb + Pb collisions, we conclude that there will be few continuum contributions above 40 GeV/c², evident from the high mass dimuon distribution published by the CMS [9], in agreement with the result shown in Fig. 7(d). The second Pb + Pb run in 2011 has 20 times more events which will help quantify the heavy flavor contribution after uncorrelated pairs are eliminated by background subtraction techniques. Their yields relative to pp collisions at the same energy can be used as a high-statistics probe of the medium properties in Pb + Pb collisions.

ACKNOWLEDGMENTS

The authors are grateful to Dr. D. K. Srivastava for many fruitful discussions. The work of R.V. was performed under the auspices of the US Department of Energy by Lawrence Livermore National Laboratory under Contract No. DE-AC52-07NA27344 and was also supported by the JET Collaboration.

[1] I. Arsene *et al.* (BRAHMS Collaboration), *Nucl. Phys. A* **757**, 1 (2005); B. B. Back *et al.* (PHOBOS Collaboration), *ibid.* **757**, 28 (2005); J. Adams *et al.* (STAR Collaboration), *ibid.* **757**, 10 (2005); K. Adcox *et al.* (PHENIX Collaboration), *ibid.* **757**, 184 (2005).
 [2] T. Matsui and H. Satz, *Phys. Lett. B* **178**, 416 (1986).
 [3] N. Armesto *et al.*, *J. Phys. G* **35**, 054001 (2008).
 [4] S. Gavin, P. L. McGaughey, P. V. Ruuskanen, and R. Vogt, *Phys. Rev. C* **54**, 2606 (1996).

[5] Z. Lin, R. Vogt, and X. N. Wang, *Phys. Rev. C* **57**, 899 (1998).
 [6] Z. Lin and R. Vogt, *Nucl. Phys. B* **544**, 339 (1999).
 [7] E. Shuryak, *Phys. Rev. C* **55**, 961 (1997).
 [8] U. Jamil and D. K. Srivastava, *J. Phys. G* **37**, 085106 (2010).
 [9] S. Chatrchyan *et al.* (CMS Collaboration), *Phys. Rev. Lett.* **106**, 212301 (2011).
 [10] S. Chatrchyan *et al.* (CMS collaboration), *JHEP* **1205**, 063 (2012); CERN Report No. CMS-HIN-10-006 (unpublished).
 [11] G. Aad *et al.* (ATLAS Collaboration), [arXiv:1012.5419](https://arxiv.org/abs/1012.5419).

- [12] A. Adare *et al.* (PHENIX Collaboration), *Phys. Rev. C* **84**, 044905 (2011).
- [13] A. Dainese *et al.* (ALICE Collaboration), *J. Phys. G* **38**, 124032 (2011).
- [14] K. Gallmeister, B. Kampfer, and O. P. Pavlenko, *Phys. Rev. C* **57**, 3276 (1998).
- [15] D. Fein, Z. Huang, P. Valerio, and I. Sarcevic, *Phys. Rev. C* **56**, 1637 (1997).
- [16] M. G. Mustafa, D. Pal, and D. K. Srivastava, *Phys. Rev. C* **57**, 889 (1998).
- [17] H. Agakishiev *et al.* (STAR Collaboration), *Phys. Rev. D* **83**, 052006 (2011); A. Adare *et al.* (PHENIX Collaboration), *Phys. Rev. Lett.* **97**, 252002 (2006).
- [18] J. Pumplin, D. R. Stump, J. Huston, H. L. Lai, P. M. Nadolsky, and W. K. Tung, *JHEP* **07** (2002) 012; D. Stump, J. Huston, J. Pumplin, W. K. Tung, H. L. Lai, S. Kuhlmann, and J. F. Owens, *J. High Energy Phys.* **10** (2003) 046.
- [19] K. J. Eskola, H. Paukkunen, and C. A. Salgado, *J. High Energy Phys.* **04** (2009) 065.
- [20] M. Cacciari, P. Nason, and R. Vogt, *Phys. Rev. Lett.* **95**, 122001 (2005).
- [21] M. L. Mangano, P. Nason, and G. Ridolfi, *Nucl. Phys. B* **373**, 295 (1992).
- [22] R. Nelson, R. Vogt, and A. D. Frawley, [arXiv:1210.4610](https://arxiv.org/abs/1210.4610) [hep-ph]; R. Vogt, R. E. Nelson, and A. D. Frawley, [arXiv:1207.6812](https://arxiv.org/abs/1207.6812).
- [23] R. Vogt, *Eur. Phys. J. Special Topics* **155**, 213 (2008).
- [24] R. Vogt, *Eur. Phys. J. C* **61**, 793 (2009).
- [25] S. Chatrchyan *et al.* (CMS Collaboration), *Phys. Rev. C* **84**, 024906 (2011).
- [26] P. Lévai and R. Vogt, *Phys. Rev. C* **56**, 2707 (1997).
- [27] R. Hamberg, W. L. van Neerven, and T. Matsuura, *Nucl. Phys. B* **359**, 343 (1991).
- [28] A. Accardi *et al.*, [arXiv:hep-ph/0308248](https://arxiv.org/abs/hep-ph/0308248).
- [29] T. Sjöstrand, S. Mrenna, and P. Skands, *J. High Energy Phys.* **05** (2006) 026.
- [30] A. D. Frawley, T. Ullrich, and R. Vogt, *Phys. Rep.* **462**, 125 (2008).
- [31] T. Sakaguchi *et al.* (PHENIX Collaboration), in Proceedings of Quark Matter 2012 [Nucl. Phys. A (to be published)].
- [32] C. Mironov *et al.* (CMS Collaboration), in Proceedings of Quark Matter 2012 [Nucl. Phys. A (to be published)].
- [33] J. D. Bjorken, *Phys. Rev. D* **27**, 140 (1983).
- [34] K. Kajantie, M. Kataja, L. McLerran, and P. V. Ruuskanen, *Phys. Rev. D* **34**, 811 (1986).
- [35] R. Vogt, B. V. Jacak, P. L. McGaughey, and P. V. Ruuskanen, *Phys. Rev. D* **49**, 3345 (1994).
- [36] C. Gale and P. Lichard, *Phys. Rev. D* **49**, 3338 (1994); C. Song, C. M. Ko, and C. Gale, *ibid.* **50**, R1827 (1994).
- [37] S. Chatrchyan *et al.* (CMS Collaboration), *JHEP* **08** (2011) 141.
- [38] S. Chatrchyan *et al.* (CMS Collaboration), *J. Instrum.* **3**, S08004 (2008).
- [39] G. Aad *et al.* (ATLAS Collaboration), *J. Instrum.* **3**, S08003 (2008).
- [40] K. Aamodt *et al.* (ALICE Collaboration), *J. Instrum.* **3**, S08002 (2008).